

ORIGINAL ARTICLE

# Neural Differentiation of Spheroids Derived from Human Induced Pluripotent Stem Cells–Mesenchymal Stem Cells Coculture

Liqing Song, MS,<sup>1</sup> Ang-Chen Tsai, PhD,<sup>1,\*</sup> Xuegang Yuan, MS,<sup>1</sup> Julie Bejoy, MS,<sup>1</sup> Sébastien Sart, PhD,<sup>2</sup> Teng Ma, PhD,<sup>1</sup> and Yan Li, PhD<sup>1</sup>

Organoids, the condensed three-dimensional (3D) tissues emerged at the early stage of organogenesis, are a promising approach to regenerate functional and vascularized organ mimics. While incorporation of heterotypic cell types, such as human mesenchymal stem cells (hMSCs) and human induced pluripotent stem cells (hiPSCs)-derived neural progenitors aid neural organ development, the interactions of secreted factors during neurogenesis have not been well understood. The objective of this study is to investigate the impact of the composition and structure of 3D hybrid spheroids of hiPSCs and hMSCs on dorsal cortical differentiation and the secretion of extracellular matrices and trophic factors *in vitro*. The hybrid spheroids were formed at different hiPSC:hMSC ratios (100:0, 75:25, 50:50, 25:75, 0:100) using direct mixing or pre-hiPSC aggregation method, which generated dynamic spheroid structure. The cellular organization, proliferation, neural marker expression, and the secretion of extracellular matrix proteins and the cytokines were characterized. The incorporation of MSCs upregulated Nestin and  $\beta$ -tubulin III expression (the dorsal cortical identity was shown by Pax6 and TBR1 expression), matrix remodeling proteins, and the secretion of transforming growth factor- $\beta$ 1 and prostaglandin E2. This study indicates that the appropriate composition and structure of hiPSC-MSC spheroids promote neural differentiation and trophic factor and matrix secretion due to the heterotypic cell–cell interactions.

**Keywords:** induced pluripotent stem cells, mesenchymal stem cells, spheroid, neural differentiation, extracellular matrix

## Introduction

CELL-BASED THERAPIES, including neural progenitor cells (NPCs) and mesenchymal stem cells (MSCs), have been explored to promote neurological recovery after transplantation, for example, spinal cord injury.<sup>1–3</sup> Transplantation of MSCs, the important source of trophic factors, was shown to modulate the environment at the transplantation site and promote axon regeneration by the secretion of anti-inflammation and antiapoptotic factors.<sup>4,5</sup> Transplantation of NPCs, on the other hand, is capable of repopulating injured tissues. Recently, deriving NPCs from human induced pluripotent stem cells (hiPSCs) was shown as an invaluable tool to study tissue regeneration,<sup>6–8</sup> because of their potential to

differentiate along neural lineages, such as neurons, astrocytes, and oligodendrocytes. Despite the promising results from both MSCs and hiPSC-derived NPCs, significant challenges remain in stem cell-based therapy. MSCs are known to have a short life span *in vivo* and the limited capacity to undergo neuronal differentiation for long-term engraftment.<sup>4</sup> On the other hand, hiPSC-derived NPCs have low engraftment and immature differentiation at the injury site, reducing efficacy outcome.<sup>9,10</sup> Toward long-term goal of overcoming these limitations, investigation of heterotypic cell–cell interactions of hiPSC-NPCs and MSCs is required.

Introducing heterotypic cell–cell interactions in the transplanted cells has shown promising outcomes. For example, transplantation of hiPSC-derived cardiomyocytes, endothelial

<sup>1</sup>Department of Chemical and Biomedical Engineering, FAMU-FSU College of Engineering, Florida State University, Tallahassee, Florida.

<sup>2</sup>Hydrodynamics Laboratory (LadHyX), Department of Mechanics, Ecole Polytechnique, CNRS-UMR7646, Palaiseau, France.

\*Current affiliation: PBS Biotech, Calle Suerte, Camarillo, California.

The preliminary results of this study were presented in 2017 annual meeting of American Institute of Chemical Engineers (AIChE), October 29–November 3, Minneapolis, Minnesota, 2017.

cells, and smooth muscle cells showed much better cell engraftment than cardiomyocytes alone in a large animal model.<sup>10,11</sup> Similarly, cotransplantation of activated Schwann cells and MSCs improved functional recovery of hindlimbs and remyelination of the injured axons with reduced formation of glial scar.<sup>12</sup> However, cotransplantations of a cell mixture in suspension lack the tissue architecture that has been shown to significantly influence secretory properties and cell survival.<sup>13</sup> Presenting the cells in three-dimensional (3D) tissue format may overcome the drawback of single-cell suspension.

Attempts have been made to transplant microtissues or spheroids to enhance cellular functional properties compared with single-cell suspension. For example, the formation of spheroids upregulates the secretion of trophic factors and cytokines for NPCs.<sup>14</sup> For MSCs, the formation of spheroids has been found to enhance the expression of antiapoptotic and anti-inflammatory proteins such as tumor necrosis factor-inducible gene 6 protein (TSG-6), STC-1, IL-6, and prostaglandin E2 (PGE-2).<sup>15–19</sup> MSC spheroids also enhance extracellular matrix (ECM) secretion, such as fibronectin and laminin,<sup>20–22</sup> which promotes NPC differentiation, prolongs cell survival, and provides better protection from nutrient/growth factor deprivation.<sup>23</sup> However, modulation of cellular microenvironment indicated by the secretion of trophic factors and ECM proteins has not been well understood during spheroid formation of multiple cell types.

Recently, Takebe *et al.* reported a generalized method to form organ buds of different types of tissues (e.g., liver, kidney, brain, etc.) using MSCs, endothelial cells, and hiPSC-derived progenitor cells.<sup>24</sup> The transplanted organ buds were shown to efficiently self-organize into multiple functional and vascularized organs, such as liver or kidney.<sup>24,25</sup> Moreover, complex 3D organoids have been created recently from hiPSCs, such as cortical or cerebral organoids,<sup>26–28</sup> to predict neurotoxicity of different drugs,<sup>29</sup> and to improve transplantation outcome.<sup>25,30</sup> By promoting the secretion of endogenous growth factors and ECM proteins, the formation of heterogeneous 3D tissue architecture recapitulates essential cellular microenvironment and cell–matrix interactions of functional tissues.<sup>14,31</sup> However, the precise role of 3D cellular organization and structural environment on organoids' biological function have been underexplored.

Given these recent advancements, this study constructs spheroids of human MSCs (hMSCs) and hiPSC-derived NPCs and investigates the impact of cell organization on the proliferation, secretion of trophic factors and ECMs, and neural differentiation *in vitro*. It is hypothesized that the heterotypic cell–cell interactions and the secretion of endogenous ECM/trophic factors in the 3D hybrid spheroids of MSCs and hiPSC-derived NPCs promote neural differentiation. Two hybrid spheroid structures fabricated by direct mixing or pre-hiPSC aggregation were assessed to understand the influence of tissue structure and the secreted trophic factors and ECMs on neural differentiation. Direct mixing enables maximum heterotypic cell–cell interactions, whereas pre-hiPSC aggregation promotes the formation of different spatial cellular organization, such as the core–shell structure. The outcome of this study advances our understanding of the interactions of multiple cell types and the modulation of extracellular microenvironment during neurogenesis toward the application of tissue organoids for *in vitro* disease modeling and cell therapy.

## Materials and Methods

### Undifferentiated human iPSC culture

Human iPSC3 cells were derived from human foreskin fibroblasts transfected with plasmid DNA encoding reprogramming factors OCT4, NANOG, SOX2, and LIN28 (kindly provided by Dr. Stephen Duncan, Medical College of Wisconsin, and Dr. David Gilbert, Department of Biological Sciences of Florida State University).<sup>32,33</sup> Human iPSC3 cells were maintained in mTeSR serum-free medium (StemCell Technologies, Inc., Vancouver, Canada) on six-well plates coated with growth factor-reduced Geltrex (Life Technologies). The cells were passaged by Accutase dissociation every 5–6 days and seeded at  $1 \times 10^6$  cells per well of a six-well plate in the presence of  $10 \mu\text{M}$  Y27632 (Sigma) for the first 24 h.<sup>34–36</sup>

### hMSC culture

Standardized frozen hMSCs from multiple donors were obtained from the Tulane Center for Gene Therapy and cultured as previously described.<sup>37,38</sup> The hMSCs were isolated from the bone marrow of healthy donors ranging in age from 19 to 49 years based on plastic adherence, negative for CD34, CD45, CD117 (all <2%) and positive for CD29, CD44, CD49c, CD90, CD105, and CD147 markers (all >95%), and possess trilineage differentiation potential upon induction *in vitro*.<sup>39,40</sup> Briefly, hMSCs were expanded at a density of  $1.7 \times 10^3$  cells/cm<sup>2</sup> using  $\alpha$ MEM (Invitrogen) medium supplemented with 10% fetal bovine serum (FBS) and 1% penicillin/streptomycin in a standard 5% CO<sub>2</sub> incubator. At ~80% confluence, adherent cells were harvested with 0.25% trypsin-EDTA (Sigma-Aldrich) and further propagated.

### Hybrid hiPSC-hMSC spheroid formation and neural differentiation

Before forming hybrid hiPSC-hMSC spheroids, undifferentiated iPSC3 cells (or preformed hiPSC aggregates) were labeled with CellTracker Green ( $2.5 \mu\text{M}$ , Life Technologies) and hMSCs were labeled with CellTracker Red ( $2.5 \mu\text{M}$ ) for 30 min. The labeling allows for imaging and tracking of the self-organization and location of two cell types after the mixing.

**Method A—direct mixing.** A total number of  $2 \times 10^4$  cells were seeded into U-bottom Ultra-low attachment (ULA) 96-well plates (Corning Incorporated, Corning, NY) at different iPSC to MSC ratios (100:0, 75:25, 50:50, 25:75, and 0:100,  $n = 3–12$ ) in neural differentiation medium composed of Dulbecco's modified Eagle's medium/Nutrient Mixture F-12 (DMEM/F-12) plus 2% B27 serum-free supplement (Life Technologies). Y27632 ( $10 \mu\text{M}$ ) was added during the seeding and removed after 24 h. At day 1, the cell aggregates were treated with dual SMAD signaling inhibitors  $10 \mu\text{M}$  SB431542 (Sigma) and  $100 \text{ nM}$  LDN193189 (Sigma) (Supplementary Fig. S1; Supplementary Data are available online at [www.liebertpub.com/tea](http://www.liebertpub.com/tea)).<sup>35,41,42</sup> After 7 days, cells were grown in neural medium without growth factors. After 14–20 days in suspension, the 3D NPC spheroids were replated onto Geltrex-coated surface and characterized for various neural markers ( $\beta$ -tubulin III, Nestin, and TBR1, etc.) and ECM remodeling proteins.

**Method B—pre-hiPSC aggregation.** Human iPSCs ( $0.5\text{--}2 \times 10^4$  cells) were seeded into U-bottom ULA 96-well plates in neural differentiation medium composed of DMEM/F-12 plus 2% B27 to construct hiPSC aggregates first (Supplementary Fig. S1). Y27632 ( $10\ \mu\text{M}$ ) was added during the seeding and removed after 24 h. The aggregates were treated with  $10\ \mu\text{M}$  SB431542 and  $100\ \text{nM}$  LDN193189. At day 5, hMSCs were added in the wells and cultured to form core-shell aggregates. For each group, a total number of  $2 \times 10^4$  cells were seeded at five different iPSC to MSC ratios (100:0, 75:25, 50:50, 25:75, and 0:100,  $n=3\text{--}12$ ). After another 7 days, cells were grown in neural medium without growth factors. At 14–20 days after the addition of MSCs, similar characterizations were performed as those for the direct mixing method.

#### Aggregate size distribution

The images of various spheroids were captured over the culture time (7 days) by a phase-contrast microscopy. The captured images were converted to binary images using ImageJ software (<http://rsb.info.nih.gov/ij>) and analyzed with the “particle analysis tool.” Through particle analysis in ImageJ software, the Feret’s diameter of each aggregate in the images can be calculated, which provides the size distribution of the aggregates.<sup>43</sup>

#### Biochemical assays

**MTT assay.** The spheroids under different conditions were incubated with  $5\ \text{mg/mL}$  3-(4,5-Dimethylthiazol-2-yl)-2,5-diphenyltetrazolium bromide (MTT; Sigma) solution at day 7 after being incorporated with MSCs. The absorbance of the samples was measured at  $490\ \text{nm}$  using a microplate reader (Bio-Rad, Richmond, CA).

**DNA assay.** The DNA content of the individual spheroids at day 7 after the addition of MSCs was determined. DNA standard was prepared by dissolving salmon testes DNA in TEX ( $10\ \text{mM}$  Tris,  $1\ \text{mM}$  EDTA,  $0.1\%$  Triton X-100 at pH 8) and a standard curve was constructed for each assay. The aggregates were lysed with  $0.1\ \text{mg/mL}$  proteinase K (Fisher Scientific, Pittsburgh, PA) at  $50^\circ\text{C}$  overnight. The lysates ( $100\ \mu\text{L}$ ) were mixed with  $100\ \mu\text{L}$  of PicoGreen (Molecular Probes, Eugene, OR) in a 96-well plate. The plate was incubated for 5 min in the dark and then read on a fluorescent plate reader (FLX800; Bioinstrument, Inc., Winooski, VT).

**LIVE/DEAD assay.** The spheroids were evaluated for viability using the Live/Dead<sup>®</sup> Staining Kit (Molecular Probes). After 7 days, the cells were incubated in DMEM-F12 containing  $1\ \mu\text{M}$  calcein AM (green) and  $2\ \mu\text{M}$  ethidium homodimer I (red) for 30 min. The samples were imaged under a fluorescent microscope.

**Enzyme-linked immunosorbent assay.** To quantify the growth factors secreted by different spheroids, culture supernatants were collected at day 4 after adding MSCs. Concentrations of prostaglandin E2 (PGE2) and transforming growth factor (TGF)- $\beta$ 1 were measured by enzyme-linked immunosorbent assay (ELISA) according to the manufacturer’s instructions (R&D Systems, Minneapolis, MN for PGE2; Life Technologies for TGF- $\beta$ 1). Briefly, the samples

were added into 96-well microplates and incubated with primary/secondary antibody solution conjugated with horseradish peroxidase (HRP) for 2–3 h. After washing, 3,3',5,5'-tetramethylbenzidine (TMB) substrate solution was added for 30 min and stopped by the stop solution. The absorbance units (AU) were measured using a microplate reader (Bio-Rad) at a wavelength of  $450\ \text{nm}$  with background subtraction at  $540\text{--}570\ \text{nm}$ . The AU values were corrected by subtracting the values of negative control stained with HRP-IgG only. The concentrations of PGE2 or TGF- $\beta$ 1 were normalized by the ratios of MSC numbers to total cell numbers.

#### Histology

For histology, the hybrid spheroids of hiPSCs (prelabeled with CellTracker Green) and hMSCs (prelabeled with CellTracker Red) were fixed in 10% formalin, dehydrated, and embedded in paraffin wax. The sections of  $10\ \mu\text{m}$  were cut and fluorescent images were captured with an Olympus IX70 microscope with MagnaFire SP 2.1B software to show the localization of hiPSCs and hMSCs.<sup>19</sup>

#### Immunocytochemistry

Briefly, the samples were fixed with 4% paraformaldehyde (PFA) and permeabilized with 0.2–0.5% Triton X-100. The samples were then blocked for 30 min and incubated with various mouse or rabbit primary antibodies (Supplementary Table S1) for 4 h. After washing, the cells were incubated with the corresponding secondary antibody: Alexa Fluor<sup>®</sup> 488 goat anti-Mouse IgG<sub>1</sub> or Alexa Fluor 488 or 594 goat anti-Rabbit IgG (Life Technologies) for 1 h. The samples were counterstained with Hoechst 33342 and visualized using a fluorescence microscope (Olympus IX70, Melville, NY) or a confocal microscope (Zeiss LSM 880). For ECM expression of laminin and Collagen IV, replated aggregates onto 0.1% gelatin-coated surface (to reduce the interference from Geltrex) were fixed and stained. MSCs were labeled with CellTracker Red for visualizing the colocalization of MSCs and ECM proteins. The images from five independent fields (800–1000 cells) were analyzed using ImageJ software. The intensity was calculated based on the area of marker of interest normalized to the nuclei, indicating the relative expression among different conditions.

#### Flow cytometry

To quantify the levels of various neural marker expression, the cells were harvested by trypsinization and analyzed by flow cytometry.<sup>44</sup> Briefly,  $1 \times 10^6$  cells per sample were fixed with 4% PFA and washed with staining buffer (2% FBS in phosphate buffered saline). The cells were permeabilized with 100% cold methanol, blocked, and then incubated with primary antibodies against Nestin and  $\beta$ -tubulin III followed by the corresponding secondary antibody Alexa Fluor 488 goat anti-Mouse IgG<sub>1</sub> (for  $\beta$ -tubulin III) and Alexa Fluor 488 goat anti-Rabbit IgG (for Nestin). The cells were acquired with BD FACSCanto<sup>™</sup> II flow cytometer (Becton Dickinson) and analyzed against isotype controls using FlowJo software.

TABLE 1. PRIMER SEQUENCE FOR TARGET GENES

Gene	Forward primer 5' to 3'	Reverse primer 5' to 3'
MMP-2	CATCGCTCAGATCCGTGGTG	GCATCAATCTTTTCCGGGAGC
MMP-3	CCATCTCTTCCTTCAGGCGT	ATGCCTCTTGGGTATCCAGC
$\beta$ -actin	GTACTCCGTGTGGATCGGCG	AAGCATTTCGGGTGGACGATGG

### Reverse transcription–polymerase chain reaction analysis

Total RNA was isolated from different cell samples using the RNeasy Mini Kit (Qiagen, Valencia, CA) according to the manufacturer's protocol followed by the treatment of the DNA-Free RNA Kit (Zymo, Irvine, CA).<sup>45</sup> Reverse transcription was carried out using 2  $\mu$ g of total RNA, anchored oligo-dT primers (Operon, Huntsville, AL), and Superscript III (Invitrogen, Carlsbad, CA) (according to the protocol of the manufacturer). Primers specific for target genes (Table 1) were designed using the software Oligo Explorer 1.2 (Gene-Link, Hawthorne, NY; Table 1). The gene  $\beta$ -actin was used as an endogenous control for normalization of expression levels. Real-time reverse transcription–polymerase chain reaction (RT-PCR) reactions were performed on an ABI7500

instrument (Applied Biosystems, Foster City, CA), using SYBR1 Green PCR Master Mix (Applied Biosystems). The amplification reactions were performed as follows: 2 min at 50°C, 10 min at 95°C, and 40 cycles of 95°C for 15 s and 55°C for 30 s, and 68°C for 30 s. Fold variation in gene expression was quantified by means of the comparative Ct method:  $2^{-(C_{t \text{ treatment}} - C_{t \text{ control}})}$ , which is based on the comparison of expression of the target gene (normalized to the endogenous control  $\beta$ -actin) between the hybrid spheroids and the spheroids of 100% hiPSCs.

### Statistical analysis

Each experiment was carried out at least three times. The representative experiments were presented and the results were expressed as mean  $\pm$  standard deviation. To assess the

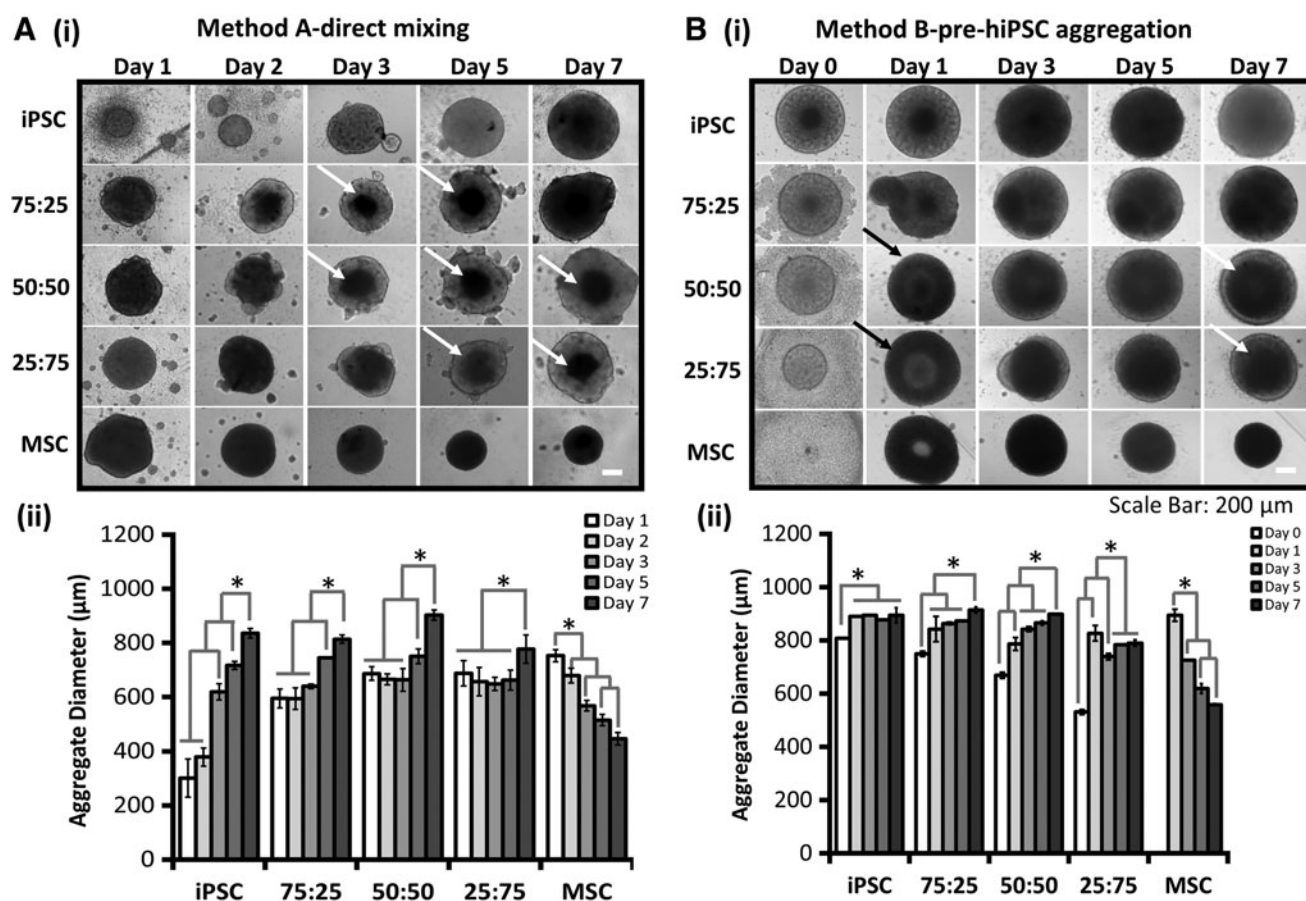


**FIG. 1.** Kinetics of hybrid hiPSC-hMSC aggregate size for direct mixing (method A) and pre-hiPSC aggregation (method B). **(A) (i)** Phase-contrast images of hiPSC-hMSC spheroid morphology at different iPSC to MSC ratios formed by direct mixing method. **(ii)** Average aggregate diameter at different days. **(B) (i)** Phase-contrast images of hiPSC-hMSC spheroid morphology at different iPSC to MSC ratios formed by pre-hiPSC aggregation method. **(ii)** Average aggregate diameter at different days ( $n=3$ ). Scale bar: 200  $\mu$ m. White arrows point to MSC core. Black arrows point to MSC shell.  $*p < 0.05$  for the different test conditions. hiPSC, human induced pluripotent stem cell; hMSC, human mesenchymal stem cell.

statistical significance, one-way analysis of variance followed by Fisher's least significant difference *post hoc* tests were performed. A *p*-value <0.05 was considered statistically significant.

## Results

### Aggregation and localization of hiPSC-hMSC hybrid spheroids

**Method A—direct mixing.** For the four hiPSC to hMSC ratios (100:0, 75:25, 50:50, and 25:75) formed by direct mixing, the cells formed structured aggregates and showed the proliferation by aggregate diameter increase (e.g., for 50:50, from  $687 \pm 25$  to  $903 \pm 19 \mu\text{m}$ ) during day 1–7 (Fig. 1Ai, ii). Most cells were viable based on LIVE/DEAD viability assay (Supplementary Fig. S2). By contrast, the size of hMSC (0:100) spheroids decreased in diameter from  $753 \pm 22$  to  $446 \pm 22 \mu\text{m}$  during day 1–7 (Fig. 1Aii). Notably, hMSC condensation in the center of spheroids was observed after day 2 (Fig. 1Ai). To confirm the observation by phase-contrast images, hMSCs were labeled with CellTracker Red and hiPSCs were labeled with CellTracker Green to visualize spatial cell distribution of two different cell types (Fig. 2A, Supplementary Fig. S3 and Supplementary Fig. S4). At day 1, hMSCs and hiPSCs were randomly distributed in the spheroids. After day 2, red hMSCs were gradually condensed in the core, whereas hiPSCs were mainly found around hMSC core. In addition, the relative area occupied by the condensed hMSCs decreased gradually from day 3 to 7.

**Method B—pre-hiPSC aggregation.** Undifferentiated hiPSCs ( $0.5\text{--}2 \times 10^4$  cells) were seeded for 5 days to form hiPSC aggregates. At day 5, hMSCs were added onto preformed hiPSC aggregates and the core-shell (hiPSC core-hMSC shell) structures were observed under different iPSC:MSC ratios (75:25, 50:50, and 25:75) (Fig. 1Bi, ii). Most cells were viable based on LIVE/DEAD viability assay (Supplementary Fig. S2). Slight increase in aggregate size was observed during day 2–7 (e.g., for 75:25 ratio, from  $843 \pm 47$  to  $914 \pm 11 \mu\text{m}$ ). Adversely, the size of hMSC (0:100) spheroids decreased in diameter from  $894 \pm 22$  to  $558 \pm 3 \mu\text{m}$  during day 1–7. In addition, iPSC-MSC hybrid aggregates (e.g., 75:25) displayed core-shell spatial distribution as demonstrated by CellTracker labeling (Fig. 2A, Supplementary Fig. S3 and Supplementary Fig. S4), with hMSCs as shell and preformed hiPSC aggregates as core. Interestingly, hMSCs showed the tendency to diffuse into the preformed hiPSC aggregates and move toward the spheroid center during the culture period (e.g., day 2 after merging, 50:50 ratio).

### Cell proliferation and metabolic activity of hiPSC-hMSC hybrid spheroids

MTT activity showed cell viability and metabolic activity of the cells in the spheroids (Fig. 3A). Higher MTT activity was observed for the hiPSC spheroids compared with the other four groups, either using the direct mixing or the pre-hiPSC aggregation methods. Spheroids of 0:100 hMSC and 25:75 iPSC-MSC generated through direct

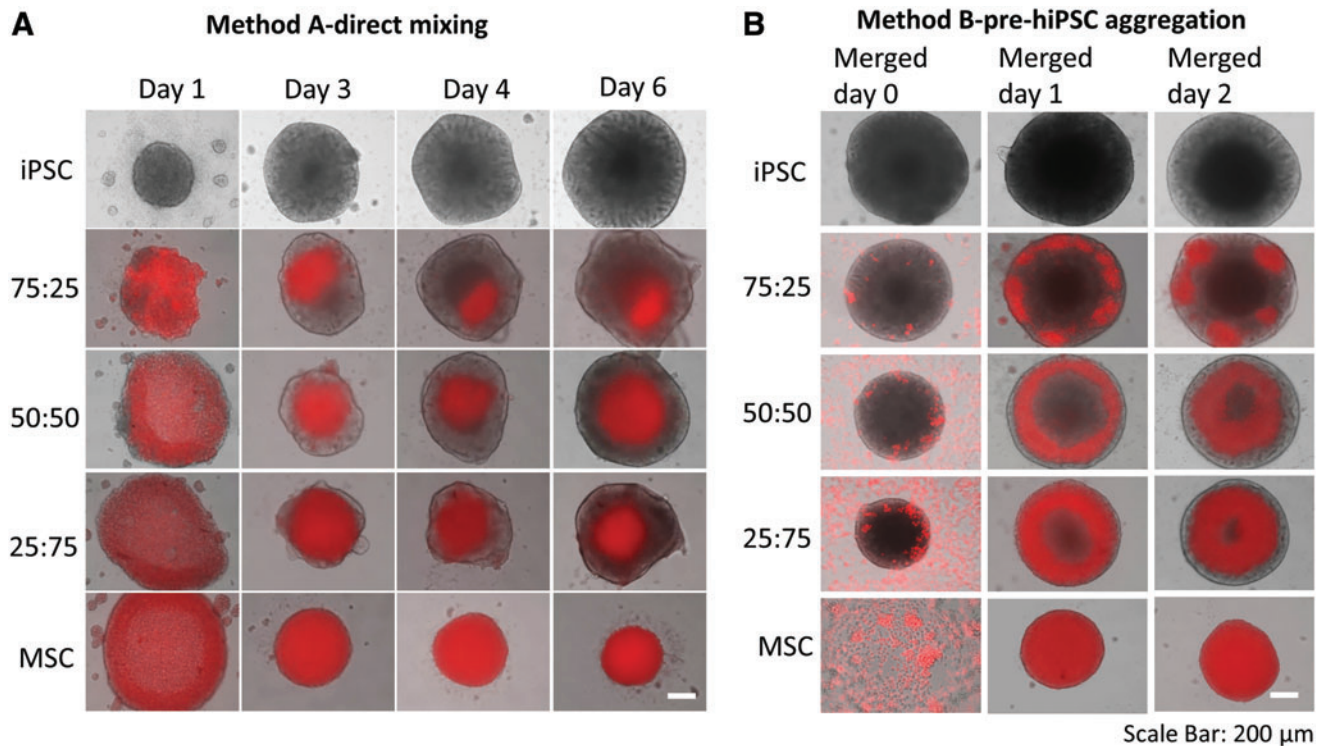
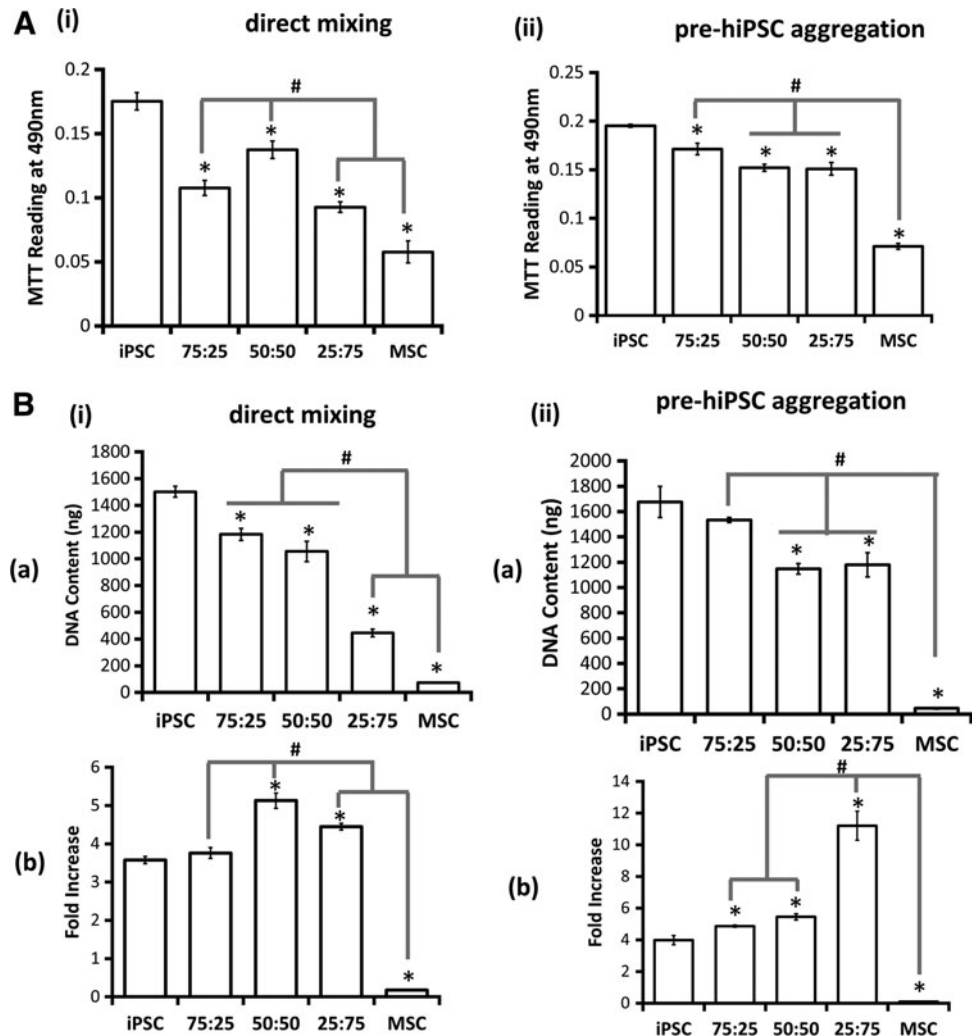


**FIG. 2.** Spatial cell distribution of hiPSC-hMSC spheroids formed by direct mixing (method A) and pre-hiPSC aggregation (method B) at different culture times. **(A)** Overlay of phase contrast images (hiPSCs) with fluorescent images (hMSCs labeled with CellTracker Red) of hiPSC-hMSC spheroids formed by direct mixing. **(B)** Overlay of phase contrast images (hiPSCs) with fluorescent images (hMSCs labeled with CellTracker Red) of hiPSC-hMSC spheroids formed by pre-hiPSC aggregation. Scale bar: 200  $\mu\text{m}$ . Color images available online at [www.liebertpub.com/tea](http://www.liebertpub.com/tea)

**FIG. 3.** Metabolic activity and DNA content of hybrid hiPSC-hMSC neural spheroids formed by different aggregation methods. (A) MTT activity: (i) direct mixing; (ii) pre-hiPSC aggregation. (B) DNA content: (i) direct mixing; (ii) pre-hiPSC aggregation. (a) Total DNA contents; (b) Fold increase based on DNA content converted to cell numbers. Assays were performed after 7 days of culture ( $n = 3$ ). \* $p < 0.05$  for the test conditions compared with the iPSC control. # $p < 0.05$  among the test conditions. MTT, 3-(4,5-Dimethylthiazol-2-yl)-2,5-diphenyltetrazolium bromide.



mixing method showed the relatively lower MTT activity compared with the other groups, whereas in the pre-hiPSC aggregation method, hybrid spheroids showed comparable MTT activity, which is much higher than hMSC spheroids.

Similarly, the DNA content of the spheroids correlated with relative abundance of hiPSCs for the direct mixing method (Fig. 3Bi-a). hiPSC spheroids (100:0) showed the highest DNA content, whereas hMSC spheroids (0:100) showed the lowest DNA content. For pre-hiPSC aggregation method, DNA content showed similar trend to that observed in direct mixing method, which is dependent of the relative ratio of iPSC in spheroids, except 25:75 iPSC-MSC, which contained comparable DNA content to 50:50 iPSC-MSC (Fig. 3Bii-a). Again, the hMSC group showed the lowest DNA content, owing to the increased apoptosis due to up-regulated caspase3/7 expression and altered mitochondria bioenergetics on 3D aggregation.<sup>46</sup> If the DNA content was converted into total cell number, the fold increase of 50:50 and 25:75 iPSC-MSC was higher than other groups for direct mixing method (Fig. 3Bi-b). For pre-iPSC aggregation, 25:75 iPSC-MSC group had the highest fold increase, indicating that this condition may promote hiPSC proliferation (Fig. 3Bii-b).

#### Expression of ECM and remodeling proteins in hybrid hiPSC-hMSC spheroids

To interrogate the influence of the coculture on ECM distribution in the hybrid spheroids, the expression of collagen type IV (Col IV) and Laminin (LN) was investigated by immunocytochemistry (Fig. 4). Both Collagen IV and laminin were homogeneously expressed in hiPSC aggregates and hMSC aggregates (Supplementary Fig. S5). In hybrid iPSC-MSC spheroids, MSCs were labeled with CellTracker Red to show colocalization with ECM proteins. Using the direct mixing method, the hybrid aggregates showed Col IV and LN expression (Fig. 4A). The group of 25:75 iPSC-MSC had higher Col IV expression, whereas LN expression seemed to increase with the ratio of hMSCs (Fig. 4C). For pre-hiPSC aggregation method, a higher level of Col IV expression was observed for the group of 25:75 iPSC-MSC. Higher LN expression was observed for the groups with higher MSC portion (Fig. 4B, D). Extensive expression of Col IV and LN was found around the hMSCs, indicating that differential hybrid spheroid structure may affect endogenous ECM dynamics.

Matrix metalloproteinases (MMPs) play a critical role in neural cell proliferation, migration, and differentiation.<sup>47</sup> In this study, MMP9 (a gelatinase) expression was observed for

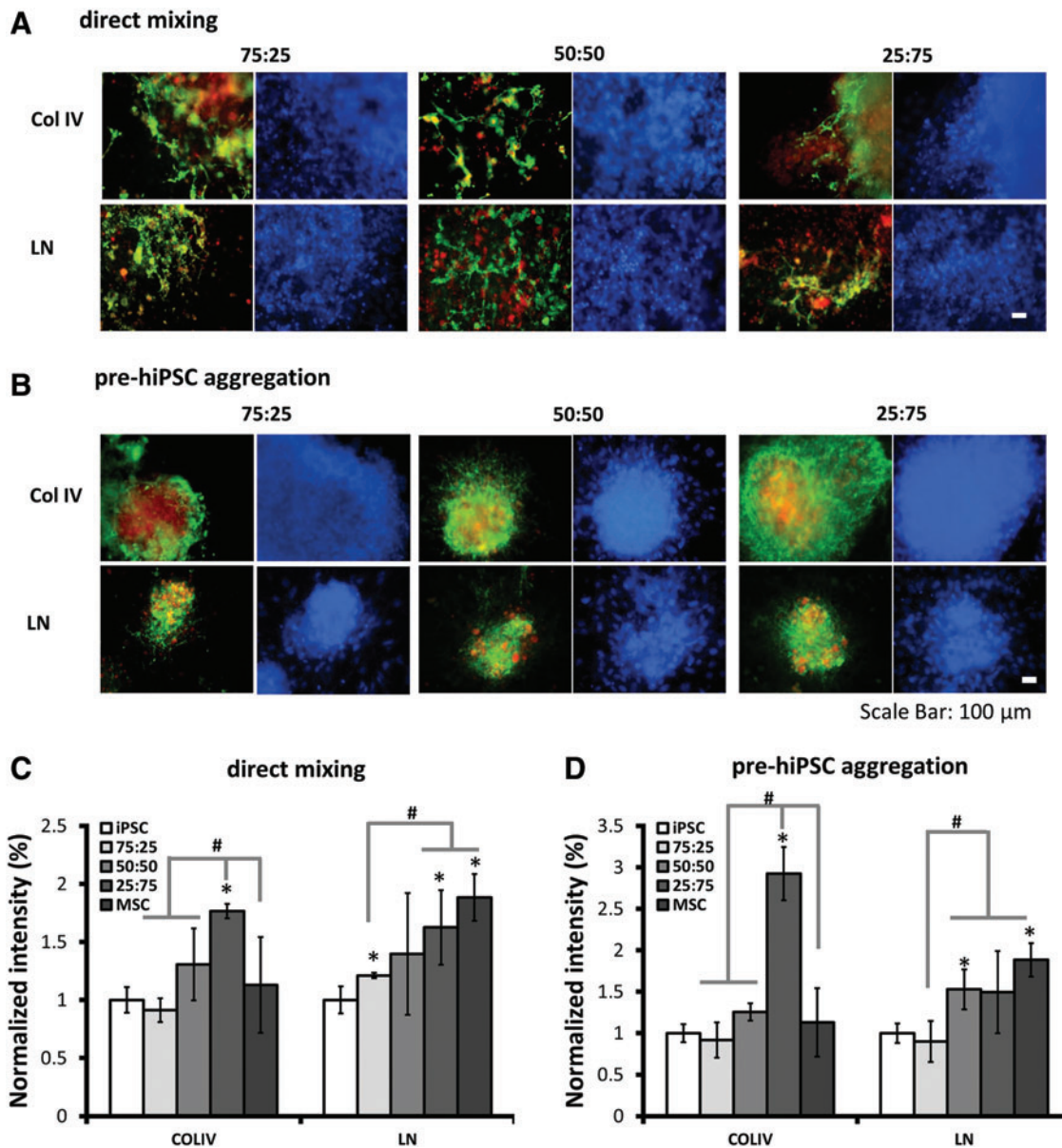


**FIG. 4.** Effects of different cell aggregation methods on collagen IV and laminin colocalization with MSCs. **(A)** Representative fluorescent images of collagen IV and laminin for hybrid spheroids generated by direct mixing method (day 14). **(B)** Representative fluorescent images of collagen IV and laminin for hybrid spheroids generated by pre-hiPSC aggregation method (day 14 after mixing). *Red:* hMSCs labeled with CellTracker Red. *Green:* Collagen IV or laminin. *Blue:* Hoechst. Scale bar: 100  $\mu$ m. **(C)** Quantification of collagen IV and laminin for spheroids generated by direct mixing method ( $n=3$ ); **(D)** Quantification of collagen IV and laminin for spheroids generated by preaggregation method ( $n=3$ ).  $*p < 0.05$  for the test conditions compared with the iPSC control.  $\#p < 0.05$  among the test conditions. Color images available online at [www.liebertpub.com/tea](http://www.liebertpub.com/tea)

spheroids of different iPSC-MSC ratios (Fig. 5A). Moreover, the gene expression of *MMP2* (another gelatinase) and *MMP3* (a broader ECM cleavage enzyme) were analyzed by RT-PCR (Fig. 5). For direct mixing method, significantly higher expression of *MMP2* (i.e.,  $39.7 \pm 1.2$ ,  $45.7 \pm 1.6$ , and  $63.3 \pm 0.5$ -fold for 75:25, 50:50, and 25:75, respectively) was observed for hybrid spheroids compared with the hiPSC spheroids (Fig. 5Bi). For *MMP3*, higher expression for hybrid spheroids (i.e.,  $7.5 \pm 0.1$ ,  $2.4 \pm 0.1$ , and  $9.4 \pm 2.7$ -fold for 75:25, 50:50, and 25:75, respectively) than 100:0 hiPSC group was observed. For pre-hiPSC aggregation method, higher expression of *MMP2* (i.e.,  $6.7 \pm 0.2$ ,  $9.4 \pm 0.9$ , fold for

75:25 and 50:50, respectively) was observed for hybrid spheroids compared with hiPSC spheroids, and *MMP3* expression was much higher (i.e.,  $23.7 \pm 0.9$ ,  $41.3 \pm 0.8$ , fold for 75:25 and 50:50, respectively) (Fig. 5Bii). These results indicate that incorporating MSCs in the hybrid spheroids up-regulated *MMP2* and *MMP3* gene expression.

*Cytokine secretion by hybrid hiPSC-hMSC spheroids*

MSCs are significant source of TGF- $\beta$ 1,<sup>48-50</sup> which exerts antiapoptotic and growth/migration-enhancing activities on NPCs.<sup>51</sup> PGE2 is a factor released by MSCs and has been

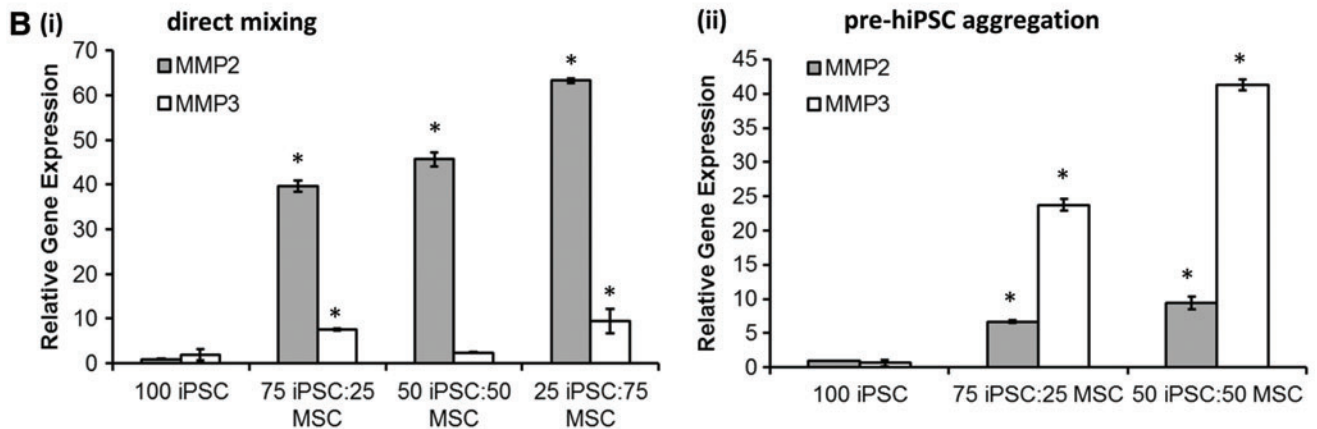
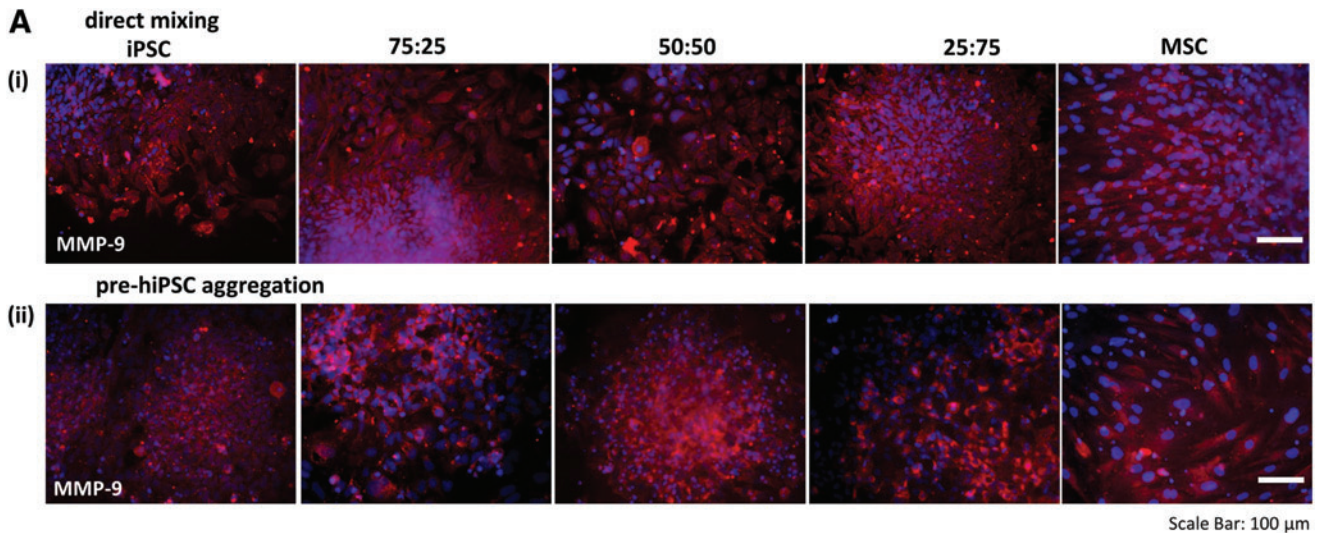


**FIG. 5.** Effects of different cell aggregation methods on the expression of ECM remodeling proteins. **(A)** Representative fluorescent images of MMP9 for spheroids (day 14) at different iPSC to MSC ratios generated by **(i)** direct mixing and **(ii)** pre-hiPSC aggregation method. *Red*: MMP9. *Blue*: Hoechst. Scale bar: 100  $\mu$ m. **(B)** Quantitative reverse transcription–polymerase chain reaction for ECM remodeling markers MMP2 and MMP3. **(i)** Direct mixing and **(ii)** pre-hiPSC aggregation method. Day 4 spheroids at different iPSC to MSC ratios were evaluated ( $n = 3$ ). \* $p < 0.05$  for the test conditions compared with the iPSC group. ECM, extracellular matrix; MMP, matrix metalloproteinase. Color images available online at [www.liebertpub.com/tea](http://www.liebertpub.com/tea)

shown to regulate multiple functions of different immune cells.<sup>52</sup> Both TGF- $\beta$ 1 and PGE2 were measured in this study. The results indicate that the 75:25 iPSC-MSC and 0:100 hMSC groups formed by direct mixing had higher normalized TGF- $\beta$ 1 concentration than the other groups (Fig. 6Ai). Using pre-hiPSC aggregation method, the normalized TGF- $\beta$ 1 concentration increases with the relative abundance of hMSCs (Fig. 6Aii). For PGE2, higher secretion was observed for 75:25 and 25:75 iPSC-MSC groups than the other groups for direct mixing method (Fig. 6Bi). For pre-hiPSC aggregation method, the normalized PGE2 concentration increases with the relative ratio of hMSCs in hybrid spheroids (Fig. 6Bii). These results indicate that incorporating MSCs at an appropriate ratio in the hybrid spheroids upregulates TGF- $\beta$ 1 and PGE2 expression compared with hiPSC spheroids.

#### Neural differentiation of hybrid hiPSC-hMSC spheroids

Neural marker expression was assessed by immunocytochemistry after 14 days of neural differentiation of hybrid spheroids. Upregulated Pax6 (forebrain neural progenitors)

and Nestin expression was observed for hybrid spheroids compared with hiPSC aggregates (Fig. 7A–D). Forebrain cortical neuron marker, TBR1, was also expressed for the hybrid spheroids at this early stage. The expression of Pax6 and TBR1 defines dorsal cortical identity of neural cells in forebrain.<sup>53</sup> Extensive expression of  $\beta$ -tubulin III, a marker for mature neurons, was observed for the aggregates of different iPSC-MSC ratios. Importantly, the neurite density of hybrid spheroids was increased with the ratio of hMSCs for pre-hiPSC aggregation method. However, little expression of Nestin, Pax6,  $\beta$ -tubulin III, and TBR1 was observed for the hMSC group. The expression of GFAP, a marker for astrocytes, was expressed for all five groups.

Neural markers, Nestin and  $\beta$ -tubulin III, were further quantified by flow cytometry (Fig. 8). For direct mixing method, Nestin expression was found higher for the hybrid spheroids (i.e.,  $47.4\% \pm 2.0\%$ ,  $45.3\% \pm 0.1\%$ , and  $49.3\% \pm 5.3\%$  for 75:25, 50:50, and 25:75, respectively) compared with the iPSC only group ( $38.7\% \pm 2.2\%$ ) (Fig. 8Ai, C). Similarly, for pre-hiPSC aggregation method, higher Nestin expression (i.e.,  $47.4\% \pm 2.0\%$ ,  $40.5\% \pm 1.9\%$ , and  $43.0\% \pm 4.2\%$  for 75:25,

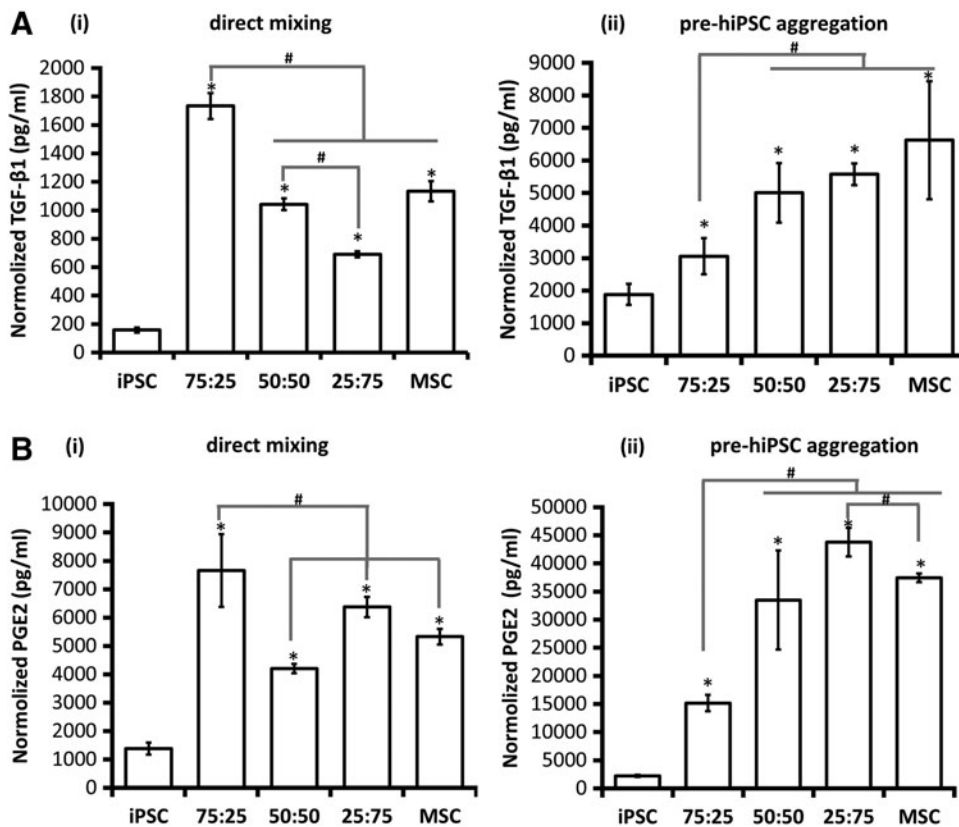


**FIG. 6.** TGF- $\beta$ 1 and PGE2 secretion by hybrid hiPSC-hMSC neural spheroids formed by different aggregation methods. (A) Concentrations of TGF- $\beta$ 1 were measured by ELISA for spheroids of different iPSC to MSC ratios at day 7 of differentiation. (i) Direct mixing and (ii) pre-hiPSC aggregation method ( $n = 3$ ). (B) Concentrations of PGE2 were measured by ELISA for spheroids of different iPSC to MSC ratios at day 7 of differentiation. (i) Direct mixing and (ii) pre-hiPSC aggregation method ( $n = 3$ ). \* $p < 0.05$  for the test conditions compared with the iPSC group. # $p < 0.05$  among the test conditions. ELISA, enzyme-linked immunosorbent assay; PGE2, prostaglandin E2; TGF, transforming growth factor.

50:50, and 25:75, respectively) was observed for the hybrid spheroids than the iPSC only group ( $35.7\% \pm 0.8\%$ ) (Fig. 8Aii, C). For  $\beta$ -tubulin III expression, higher levels were observed for hybrid spheroids (i.e.,  $59.0\% \pm 4.0\%$ ,  $56.3\% \pm 9.8\%$ , and  $48.6\% \pm 2.1\%$  for 75:25, 50:50, and 25:75, respectively) than the iPSC only group ( $42.4\% \pm 1.4\%$ ) using direct mixing method (Fig. 8Bi, D). Similarly, for pre-hiPSC aggregation method,  $\beta$ -tubulin III expression was higher for hybrid spheroids (i.e.,  $52.5\% \pm 0.8\%$ ,  $73.2\% \pm 6.6\%$ , and  $61.4\% \pm 20.8\%$  for 75:25, 50:50, and 25:75, respectively) than the iPSC only group ( $44.3\% \pm 5.7\%$ ) (Fig. 8Bii, D).

## Discussion

The microenvironment of neuropermissive matrix, trophic factors, and adherent molecules plays critical roles in neural tissue regeneration by forming guiding strands that direct axon regeneration.<sup>4,54</sup> The cocultivation of MSCs with PSCs in 2-D promotes neural differentiation through synergistic paracrine interactions.<sup>55</sup> However, it remains unclear if direct cell-cell interactions take part in the neuropromoting effect of the coculture. On the other hand, the formation of 3D spheroids significantly enriched the secreted ECM proteins and growth factors with potent neurogenic functions (e.g., laminin and vascular endothelial growth factor [VEGF]).<sup>14,21,56</sup> Moreover, the arrangement and the interactions between stromal cells and PSCs is changed in 3D aggregates, leading to the modulation of cell-cell contacts' downstream signaling (e.g., Notch).<sup>57</sup> However, their influences on neural differentiation are largely unknown. Therefore, this study investigates the influence of heterotypic cell-cell interactions on neural differentiation and the

secretory functions of both cell populations, which have been poorly understood to date.

### Dynamic regulation of heterotypic cell-cell interactions

*In vivo*, the complex tissues are integrated in a spatially restricted manner and provide dictatorial signals that organize sequential developmental events with tissue-specific function.<sup>58</sup> The *in vitro* culture aims to mimic the similar organization events, in which cells reorganize to minimize the surface energy of the 3D structure according to differential adhesion hypothesis (DAH) and the differential surface tension hypothesis.<sup>17</sup> In this study, hMSC condensation in the core of hybrid aggregates was observed during culture period. In direct mixing, different cell populations self-organize based on their relative degree of adhesiveness, and hMSCs may have stronger homotypic cell-cell interactions than hiPSC-NPCs. The observed core-shell spheroids are consistent with DAH predictions, which suggest that hMSCs with greater cohesiveness formed a core. In contrast, when mixed with preaggregated hiPSCs, hMSCs were found at the outer layer of the spheroids initially (with iPSC-NPC core and hMSCs as shell), which suggests that differential cell cortical tension between hiPSC-NPCs and hMSCs may dominate over homotypic cadherin-cadherin interactions. After the addition of MSCs, the formation of a cohesive hybrid spheroid requires additional energy input to destabilize the hiPSC-NPC aggregate structure, which results in prolonged kinetics to reach energy equilibrium. Therefore, mixing monodispersed hMSCs and precultured hiPSC spheroids suggested a potential method to control relative cell position in complex heterotypic 3D spheroids.

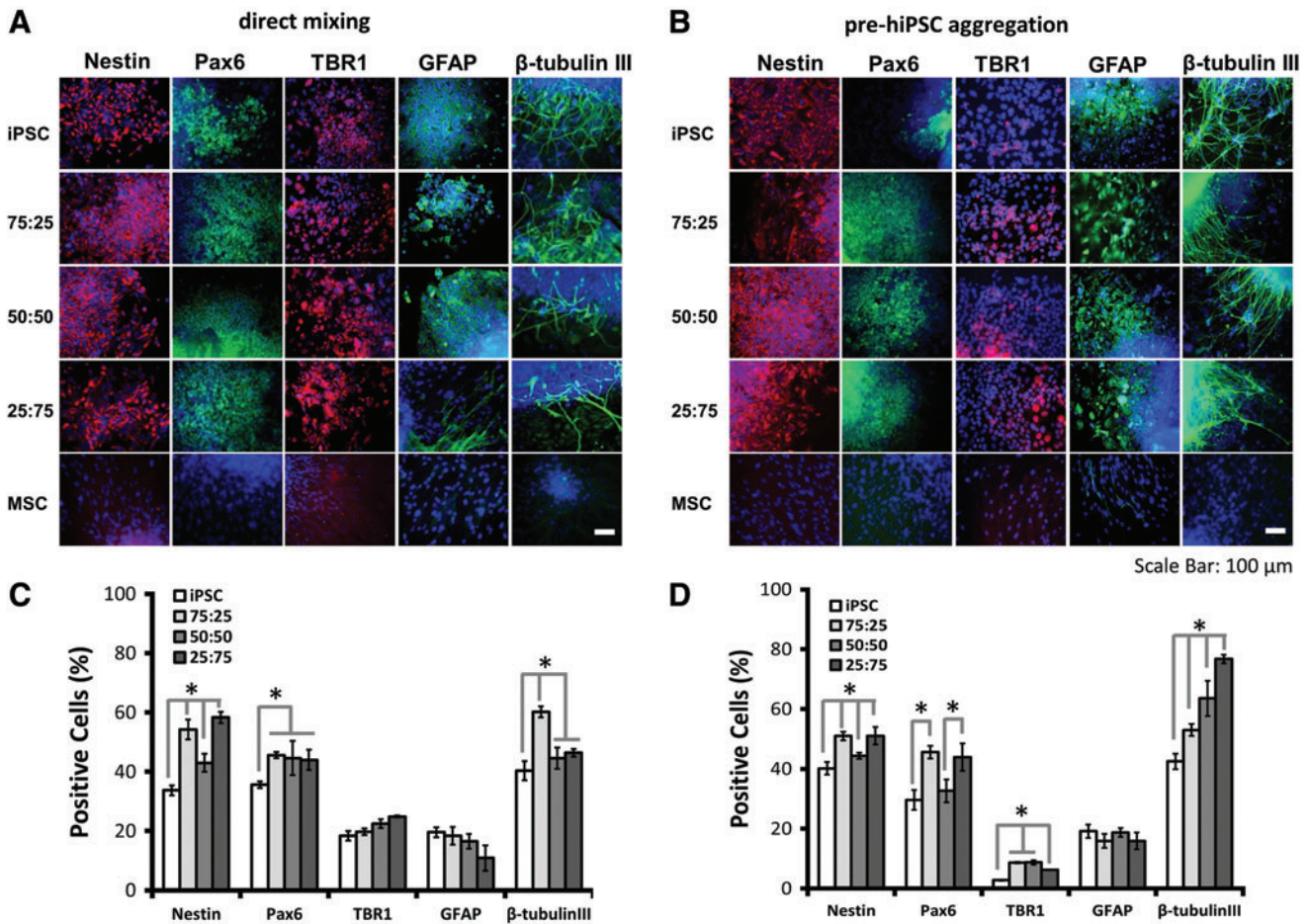


**FIG. 7.** Neural marker expression of hybrid hiPSC-hMSC neural spheroids formed by different aggregation methods. Day 14 spheroids were replated for 3 days and immunocytochemistry was performed. **(A)** Representative fluorescent images of neural markers for hybrid spheroids formed by direct mixing method. **(B)** Representative fluorescent images of neural markers for hybrid spheroids formed by pre-hiPSC aggregation method. Neural markers include: Nestin (red)/Hoechst (blue) (progenitors), Pax6 (green)/Hoechst (blue) (forebrain neural progenitors), TBR1 (red)/Hoechst (blue) (cortical neural progenitors), GFAP (green)/Hoechst (blue) (astrocytes), and  $\beta$ -tubulin III (green)/Hoechst (blue) (neurons). Scale bar: 100  $\mu$ m. **(C)** Quantification of neural marker expression for direct mixing method; **(D)** Quantification of neural marker expression for pre-hiPSC aggregation method. \* $p < 0.05$  between the test conditions. Color images available online at [www.liebertpub.com/tea](http://www.liebertpub.com/tea)

The formation of heterotypic spheroids with different ratios was reported to not influence the cell sorting process and the final state of self-assembly.<sup>59</sup> However, the kinetics to reach the surface energy balance is altered and correlated with the relative abundance of the two cell types.<sup>59</sup> Consistently, it was found that the 75:25 group required more time to reach the equilibrium than the 25:75 group for pre-hiPSC aggregation method. In addition, differential proliferation rate between the hiPSCs and hMSCs changed the ratio of mixed cell population over time and consequently the surface energy balance.<sup>60</sup> In direct mixing, cell proliferation had minimal influence on the final state, since surface energy-minimized 3D structure was already reached by day 2. However, in the preaggregation methods, the sustained imbalance in the cell ratio induced by the proliferation of hiPSCs in the 75:25 and 25:75 groups inversely correlated with the time required to reach the surface energy equilibrium. Taken together, the results suggest that both cell mixing ratios and aggregation methods regulate the

kinetics of heterospheroid formation. The direct mixing method resulted in spheroids with an outer hiPSC layer and hMSC core. By contrast, the preaggregation method enabled a metastable surface energy status, where a ring of hMSCs covers hiPSCs.

#### *The role of ECM secretion in heterotypic cell-cell interactions*

HMSCs are an important source of ECM. The culture of hMSCs as spheroids was reported to enhance the secretion of ECM proteins such as fibronectin and laminin.<sup>20-22</sup> Similarly, PSC-derived NPC aggregates produce fibronectin, Col IV, and vitronectin.<sup>44</sup> Using the direct mixing method, Col IV and LN are distributed evenly within the heterotypic spheroids, suggesting that hMSCs and hiPSC-NPCs contribute cooperatively to the structure of heterotypic spheroids. In the pre-hiPSC aggregation method, a higher level of Col IV was observed in the aggregates formed with the

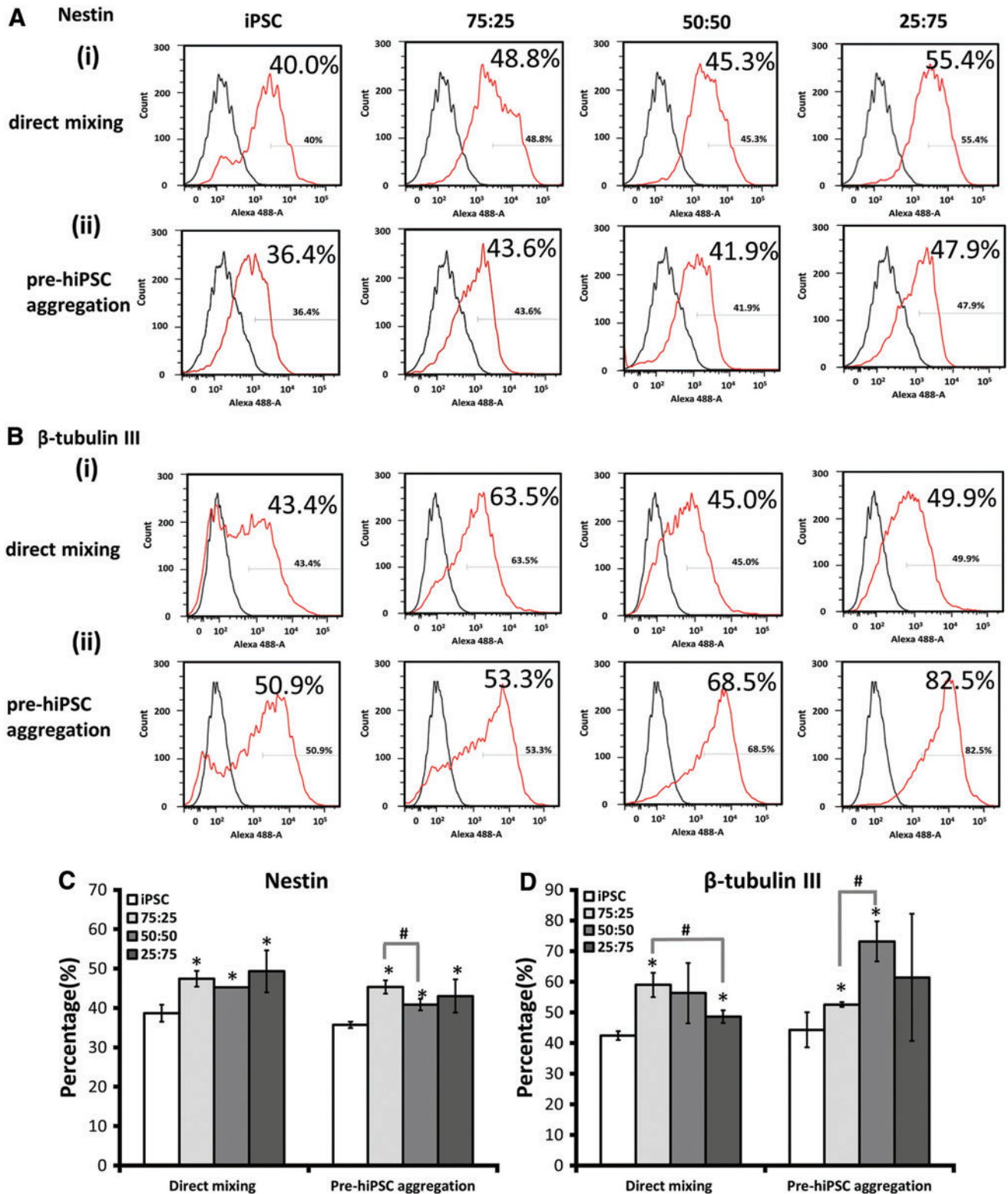


**FIG. 8.** Nestin and  $\beta$ -tubulin III expression quantified by flow cytometry for hybrid hiPSC-hMSC spheroids formed by different aggregation methods. Flow cytometry histograms for spheroids formed at different iPSC to MSC ratios (100:0, 75:25, 50:50, and 25:75) at day 14 of neural differentiation. **(A)** Nestin. **(i)** Direct mixing method; **(ii)** pre-hiPSC aggregation method. **(B)**  $\beta$ -tubulin III. **(i)** Direct mixing method; **(ii)** pre-hiPSC aggregation method. *Black line:* Negative control; *red line:* Nestin or  $\beta$ -tubulin III. **(C)** Flow cytometry quantification of Nestin ( $n=3$ ). **(D)** Flow cytometry quantification of  $\beta$ -tubulin III ( $n=3$ ). \* $p < 0.05$  for the test conditions compared with the iPSC control. # $p < 0.05$  among the test conditions. Color images available online at [www.liebertpub.com/tea](http://www.liebertpub.com/tea)

higher hMSC percentage (25:75), indicating that the invasion of hMSC into the preformed hiPSC spheroids requires significant ECM remodeling.

MMPs are a group of proteolytic enzymes, which mediate ECM degradation and remodeling.<sup>47</sup> The cocultivation of hiPSCs and hMSCs in heterotypic spheroids revealed differential regulation of MMP-2 and MMP-3, and that MSCs are the major contributor to the MMP expression (Fig. 5). In the direct mixing method, MMP-2 expression increased with the portion of hMSCs in hybrid spheroids, which may contribute to the MSC condensation in the core of the hybrid spheroids. On the other hand, for the preaggregation method, a correlation between MMP-3 expression and the relative abundance of hMSCs in the heterotypic spheroids were observed, suggesting an important contribution of MMP-3 to facilitate hMSC migration and invasion in preaggregated hiPSC-NPCs.

#### *The role of cytokine secretion in heterotypic cell–cell interactions*

HMSCs and NPCs are important sources of soluble molecules, which play significant roles in autocrine and paracrine effects in 3D cultures. For instance, MSC spheroids formed through hanging drop or forced aggregation have been found to enhance the expression of antiapoptotic and anti-inflammatory proteins such as TSG-6 and STC-1, anti-cancer molecules such as IL-24 and CD82,<sup>15–18</sup> as well as the angiogenic factors such as VEGF.<sup>61,62</sup> Similarly, NPCs secrete platelet-derived growth factor, bone morphogenic protein, epidermal growth factor, basic fibroblast growth factor, and Wnt ligands, which regulate proliferation and promote early differentiation into neuronal and glial lineages.<sup>63</sup>

In this study, the presence of MSCs (e.g., 75:25 iPSC-MS) in hybrid spheroids showed significantly higher secretion of PGE-2, either using direct mixing or the preaggregation method compared with the hiPSC only group. In addition, the secretion of TGF- $\beta$ 1 increased with the relative abundance of hMSCs. Mild hypoxia or autophagy may be involved in the enhanced secretion of PGE-2 and TGF- $\beta$ 1 by hMSCs.<sup>64,65</sup> The specific location of hMSCs (i.e., the core) in the hybrid aggregate may be linked with the increased soluble factor secretion. Moreover, nitric oxide is a potent inducer of PGE-2 secretion by NPCs, which can also be activated by the hypoxia induced in large aggregates.<sup>66</sup> In addition, PGE-2 induces profound ECM remodeling mediated by the induction of MMPs,<sup>67</sup> which play a role in the growth factor secretion by hMSCs.<sup>68</sup> Thus, it is likely that PGE-2 secretion precedes ECM remodeling in the hybrid spheroids.

The molecular mechanisms of the increased expression of PGE-2 in hMSC aggregates may involve the regulation of NF- $\kappa$ B upon aggregation (e.g., through caspase and IL-1 $\alpha$  signaling).<sup>69</sup> Indeed, the inhibition of NF- $\kappa$ B signaling by small molecules (e.g., QNZ, a NF- $\kappa$ B inhibitor) was found to abrogate PGE-2 secretion in hMSC aggregates.<sup>69</sup> Of interest, it was found that the secretion of TGF- $\beta$ 1 and PGE-2 in neural progenitors is mediated by inflammatory molecules (i.e., TNF- $\alpha$  and/or IFN- $\gamma$ ), which triggers the NF- $\kappa$ B signaling.<sup>70</sup> Consequently, the increased secretion of PGE-2 suggested cooperative role between hMSCs and hiPSC-NPCs in the hybrid spheroids, which may be promoted by the activation of NF- $\kappa$ B signaling in the two cell types.

#### *The role of MSC in neural differentiation*

MSC-derived ECM proteins can enhance neural differentiation, prolong cell survival, and provide better protection from nutrient and growth factor deprivation.<sup>23</sup> However, modulation of cellular microenvironment indicated by the secretion of trophic factors and ECM proteins has not been well understood during hybrid spheroid formation. In this study, it was found that hiPSCs are the main cell type capable of cortical neuronal differentiation in the hybrid spheroids, while the expression of neural markers was low in hMSCs. Using direct mixing and preaggregation methods, the presence of hMSCs in the hybrid spheroids promoted neuronal differentiation (i.e., Nestin and  $\beta$ -tubulin III expression) compared with the hiPSC only group. Our differentiation procedure should promote neurons of dorsal cortical identity of forebrain (expressing markers Pax6 and TBR1).<sup>42,53</sup> These results suggest an important paracrine role of hMSCs for the regulation of hiPSC fates, which are mediated by direct interactions between the two cell types.

ECM remodeling may also be an important contributing factor that enhances neural differentiation. Hybrid spheroids composed of a higher ratio of hMSC-promoted MMP expression, which is characterized by a balance between degradation and neosynthesis of structural ECM proteins. Indeed, the formation of hMSC aggregates upregulates the expression of several types of MMPs (MMP-2, -9, and -1/13).<sup>71</sup> Moreover, activation of MMPs was reported to enhance stem cell differentiation toward neuronal lineage, through the NF- $\kappa$ B signaling.<sup>72</sup> On the other hand, the formation of hMSC spheroids was also reported to enhance ECM secretion.<sup>20–22</sup> The secretion of ECM proteins by hMSCs such as collagen IV and laminin in the heterotypic spheroids may affect hiPSC fate and promote neuronal differentiation.

Previous studies demonstrated that the secretome of hMSCs also promoted neural differentiation of NPCs.<sup>73,74</sup> In particular, TGF- $\beta$ 1 exerts antiapoptotic and growth/migration-enhancing activities on NPCs through SMAD2 (for growth and migration) and ERK1/2 (for antiapoptotic behavior) signaling,<sup>51</sup> which can promote  $\beta$ -tubulin III expression.<sup>75</sup> In our study, TGF- $\beta$ 1 may partially contribute to the enhanced neuronal differentiation of hiPSCs. Alternatively, PGE-2 or proinflammatory environment was demonstrated to promote neuronal differentiation, through the regulation of the NF- $\kappa$ B signaling.<sup>76,77</sup> These observations are consistent with results of the present study, which demonstrate that the presence of hMSC in the hybrid spheroid promotes the levels of Nestin and  $\beta$ -tubulin III.

#### **Conclusions**

The modulation of heterotypic interactions between hMSCs and hiPSCs, imposed by different mixing methods and relative population abundance, dynamically regulates cellular self-organization in the hybrid dorsal cortical spheroids. The dynamics of cellular spatial organization in the hybrid spheroids promote the gene expression of ECM remodeling proteins and the secretion of PGE-2 and TGF- $\beta$ 1. The microenvironment changes induced by ECM and soluble factor secretion (higher at 25:75 iPSC to MSC ratio in general) due to MSC-hiPSC interactions cooperatively promote cortical neural differentiation of hiPSCs.

## Acknowledgments

The authors thank Ms. Ruth Didier of FSU Department of Biomedical Sciences for her help with flow cytometry analysis, Dr. Brian K. Washburn and Kristina Poduch in FSU Department of Biological Sciences for their help with RT-PCR analysis, Dr. Stephen Duncan at Medical College of Wisconsin and Dr. David Gilbert in FSU Department of Biological Sciences for human iPSC3 cells. This work is supported by FSU start up fund, FSU Bridge Grant, NSF Career Award (No. 1652992 to Y.L.), and by NIH R03EB020770 (Y.L.). The content is solely the responsibility of the authors and does not necessarily represent the official views of the National Institutes of Health.

## Disclosure Statement

No competing financial interests exist.

## References

- Ronaghi, M., Erceg, S., Moreno-Manzano, V., and Stojkovic, M. Challenges of stem cell therapy for spinal cord injury: human embryonic stem cells, endogenous neural stem cells, or induced pluripotent stem cells? *Stem Cells* **28**, 93, 2010.
- Rowland, J.W., Hawryluk, G.W., Kwon, B., and Fehlings, M.G. Current status of acute spinal cord injury pathophysiology and emerging therapies: promise on the horizon. *Neurosurg Focus* **25**, E2, 2008.
- Phinney, D.G., and Prockop, D.J. Concise review: mesenchymal stem/multipotent stromal cells: the state of transdifferentiation and modes of tissue repair—current views. *Stem Cells* **25**, 2896, 2007.
- Wright, K.T., El Masri, W., Osman, A., Chowdhury, J., and Johnson, W.E. Concise review: Bone marrow for the treatment of spinal cord injury: mechanisms and clinical applications. *Stem Cells* **29**, 169, 2011.
- Joyce, N., Annett, G., Wirthlin, L., Olson, S., Bauer, G., and Nolte, J.A. Mesenchymal stem cells for the treatment of neurodegenerative disease. *Regen Med* **5**, 933, 2010.
- Nori, S., Okada, Y., Yasuda, A., *et al.* Grafted human-induced pluripotent stem-cell-derived neurospheres promote motor functional recovery after spinal cord injury in mice. *Proc Natl Acad Sci U S A* **108**, 16825, 2011.
- All, A.H., Gharibani, P., Gupta, S., *et al.* Early intervention for spinal cord injury with human induced pluripotent stem cells oligodendrocyte progenitors. *PLoS One* **10**, e0116933, 2015.
- Salewski, R.P., Mitchell, R.A., Li, L., *et al.* Transplantation of induced pluripotent stem cell-derived neural stem cells mediate functional recovery following thoracic spinal cord injury through remyelination of axons. *Stem Cells Transl Med* **4**, 743, 2015.
- Pouya, A., Satarian, L., Kiani, S., Javan, M., and Baharvand, H. Human induced pluripotent stem cells differentiation into oligodendrocyte progenitors and transplantation in a rat model of optic chiasm demyelination. *PLoS One* **6**, e27925, 2011.
- Ye, L., Chang, Y.H., Xiong, Q., *et al.* Cardiac repair in a porcine model of acute myocardial infarction with human induced pluripotent stem cell-derived cardiovascular cells. *Cell Stem Cell* **15**, 750, 2014.
- Burridge, P.W., Metzler, S.A., Nakayama, K.H., *et al.* Multi-cellular interactions sustain long-term contractility of human pluripotent stem cell-derived cardiomyocytes. *Am J Transl Res* **6**, 724, 2014.
- Ban, D.X., Ning, G.Z., Feng, S.Q., *et al.* Combination of activated Schwann cells with bone mesenchymal stem cells: the best cell strategy for repair after spinal cord injury in rats. *Regen Med* **6**, 707, 2011.
- Kelm, J.M., and Fussenegger, M. Scaffold-free cell delivery for use in regenerative medicine. *Adv Drug Deliv Rev* **62**, 753, 2010.
- Lai, Y., Asthana, A., Cheng, K., and Kisaalita, W.S. Neural cell 3D microtissue formation is marked by cytokines' up-regulation. *PLoS One* **6**, e26821, 2011.
- Bartosh, T.J., Ylostalo, J.H., Mohammadipoor, A., *et al.* Aggregation of human mesenchymal stromal cells (MSCs) into 3D spheroids enhances their antiinflammatory properties. *Proc Natl Acad Sci U S A* **107**, 13724, 2010.
- Frith, J.E., Thomson, B., and Genever, P.G. Dynamic three-dimensional culture methods enhance mesenchymal stem cell properties and increase therapeutic potential. *Tissue Eng Part C Methods* **16**, 735, 2010.
- Sart, S., Tsai, A.-C., Li, Y., and Ma, T. Three-dimensional aggregates of mesenchymal stem cells: cellular mechanisms, biological properties, and applications. *Tissue Eng Part B Rev* **20**, 365, 2014.
- Kim, J., and Ma, T. Endogenous extracellular matrices enhance human mesenchymal stem cell aggregate formation and survival. *Biotechnol Prog* **29**, 441, 2013.
- Tsai, A.C., Liu, Y., Yuan, X., and Ma, T. Compaction, fusion, and functional activation of three-dimensional human mesenchymal stem cell aggregate. *Tissue Eng Part A* **21**, 1705, 2015.
- Lee, W.Y., Chang, Y.H., Yeh, Y.C., *et al.* The use of injectable spherically symmetric cell aggregates self-assembled in a thermo-responsive hydrogel for enhanced cell transplantation. *Biomaterials* **30**, 5505, 2009.
- Wang, C.C., Chen, C.H., Hwang, S.M., *et al.* Spherically symmetric mesenchymal stromal cell bodies inherent with endogenous extracellular matrices for cellular cardiomyoplasty. *Stem Cells* **27**, 724, 2009.
- Cheng, N.C., Wang, S., and Young, T.H. The influence of spheroid formation of human adipose-derived stem cells on chitosan films on stemness and differentiation capabilities. *Biomaterials* **33**, 1748, 2012.
- Aizman, I., Tate, C.C., McGrogan, M., and Case, C.C. Extracellular matrix produced by bone marrow stromal cells and by their derivative, SB623 cells, supports neural cell growth. *J Neurosci Res* **87**, 3198, 2009.
- Takebe, T., Enomura, M., Yoshizawa, E., *et al.* Vascularized and complex organ buds from diverse tissues via mesenchymal cell-driven condensation. *Cell Stem Cell* **16**, 556, 2015.
- Takebe, T., Sekine, K., Enomura, M., *et al.* Vascularized and functional human liver from an iPSC-derived organ bud transplant. *Nature* **499**, 481, 2013.
- Lancaster, M.A., and Knoblich, J.A. Organogenesis in a dish: modeling development and disease using organoid technologies. *Science* **345**, 1247125, 2014.
- Pasca, A.M., Sloan, S.A., Clarke, L.E., *et al.* Functional cortical neurons and astrocytes from human pluripotent stem cells in 3D culture. *Nat Methods* **12**, 671, 2015.
- Birey, F., Andersen, J., Makinson, C.D., *et al.* Assembly of functionally integrated human forebrain spheroids. *Nature* **545**, 54, 2017.
- Schwartz, M.P., Hou, Z., Propson, N.E., *et al.* Human pluripotent stem cell-derived neural constructs for predicting neural toxicity. *Proc Natl Acad Sci U S A* **112**, 12516, 2015.

30. Yin, X., Mead, B.E., Safaee, H., Langer, R., Karp, J.M., and Levy, O. Engineering stem cell organoids. *Cell Stem Cell* **18**, 25, 2016.
31. Woodford, C., and Zandstra, P.W. Tissue engineering 2.0: guiding self-organization during pluripotent stem cell differentiation. *Curr Opin Biotechnol* **23**, 810, 2012.
32. Si-Tayeb, K., Noto, F.K., Sepac, A., *et al.* Generation of human induced pluripotent stem cells by simple transient transfection of plasmid DNA encoding reprogramming factors. *BMC Dev Biol* **10**, 81, 2010.
33. Si-Tayeb, K., Noto, F.K., Nagaoka, M., *et al.* Highly efficient generation of human hepatocyte-like cells from induced pluripotent stem cells. *Hepatology* **51**, 297, 2010.
34. Yan, Y., Martin, L., Bosco, D., *et al.* Differential effects of acellular embryonic matrices on pluripotent stem cell expansion and neural differentiation. *Biomaterials* **73**, 231, 2015.
35. Yan, Y., Bejoy, J., Xia, J., Guan, J., Zhou, Y., and Li, Y. Neural patterning of human induced pluripotent stem cells in 3-D cultures for studying biomolecule-directed differential cellular responses. *Acta Biomater* **42**, 114, 2016.
36. Yan, Y., Li, Y., Song, L., Zeng, C., and Li, Y. Pluripotent stem cell expansion and neural differentiation in 3-D scaffolds of tunable Poisson's ratio. *Acta Biomater* **49**, 192, 2017.
37. Zhao, F., and Ma, T. Perfusion bioreactor system for human mesenchymal stem cell tissue engineering: dynamic cell seeding and construct development. *Biotechnol Bioeng* **91**, 482, 2005.
38. Grayson, W.L., Ma, T., and Bunnell, B. Human mesenchymal stem cells tissue development in 3D PET matrices. *Biotechnol Prog* **20**, 905, 2004.
39. Munoz, N., Kim, J., Liu, Y., Logan, T.M., and Ma, T. Gas chromatography-mass spectrometry analysis of human mesenchymal stem cell metabolism during proliferation and osteogenic differentiation under different oxygen tensions. *J Biotechnol* **169**, 95, 2014.
40. Grayson, W.L., Zhao, F., Izadpanah, R., Bunnell, B., and Ma, T. Effects of hypoxia on human mesenchymal stem cell expansion and plasticity in 3D constructs. *J Cell Physiol* **207**, 331, 2006.
41. Bejoy, J., Song, L., Zhou, Y., and Li, Y. Wnt/Yes-Associated protein interactions during neural tissue patterning of human induced pluripotent stem cells. *Tissue Eng Part A* 2017 [Epub ahead of print]; DOI: 10.1089/ten.TEA.2017.0153.
42. Yan, Y., Song, L., Madinya, J., Ma, T., and Li, Y. Derivation of cortical spheroids from human induced pluripotent stem cells in a suspension bioreactor. *Tissue Eng Part A* 2017 [Epub ahead of print]; DOI: 10.1089/ten.TEA.2016.0400.
43. Sart, S., Calixto Bejarano, F., Baird, M.A., *et al.* Intracellular labeling of mouse embryonic stem cell-derived neural progenitor aggregates with micron-sized particles of iron oxide. *Cytherapy* **17**, 98, 2015.
44. Sart, S., Ma, T., and Li, Y. Extracellular matrices decellularized from embryonic stem cells maintained their structure and signaling specificity. *Tissue Eng Part A* **20**, 54, 2014.
45. Song, L., Wang, K., Li, Y., and Yang, Y. Nanotopography promoted neuronal differentiation of human induced pluripotent stem cells. *Colloids Surf B Biointerfaces* **148**, 49, 2016.
46. Kelm, J.M., Breitbach, M., Fischer, G., *et al.* 3D micro-tissue formation of undifferentiated bone marrow mesenchymal stem cells leads to elevated apoptosis. *Tissue Eng Part A* **18**, 692, 2011.
47. Ethell, I.M., and Ethell, D.W. Matrix metalloproteinases in brain development and remodeling: synaptic functions and targets. *J Neurosci Res* **85**, 2813, 2007.
48. Robinson, A.P., Foraker, J.E., Ylostalo, J., and Prockop, D.J. Human stem/progenitor cells from bone marrow enhance glial differentiation of rat neural stem cells: a role for transforming growth factor beta and Notch signaling. *Stem Cells Dev* **20**, 289, 2011.
49. Hawryluk, G.W., Mothe, A.J., Chamankhah, M., Wang, J., Tator, C., and Fehlings, M.G. In vitro characterization of trophic factor expression in neural precursor cells. *Stem Cells Dev* **21**, 432, 2012.
50. Montes, R., Ligeró, G., Sanchez, L., *et al.* Feeder-free maintenance of hESCs in mesenchymal stem cell-conditioned media: distinct requirements for TGF-beta and IGF-II. *Cell Res* **19**, 698, 2009.
51. Park, S.M., Jung, J.S., Jang, M.S., Kang, K.S., and Kang, S.K. Transforming growth factor-beta1 regulates the fate of cultured spinal cord-derived neural progenitor cells. *Cell Prolif* **41**, 248, 2008.
52. Kalinski, P. Regulation of immune responses by prostaglandin E2. *J Immunol* **188**, 21, 2012.
53. Bagley, J.A., Reumann, D., Bian, S., Levi-Strauss, J., and Knoblich, J.A. Fused cerebral organoids model interactions between brain regions. *Nat Methods* **14**, 743, 2017.
54. Hofstetter, C.P., Schwarz, E.J., Hess, D., *et al.* Marrow stromal cells form guiding strands in the injured spinal cord and promote recovery. *Proc Natl Acad Sci U S A* **99**, 2199, 2002.
55. Joshi, R., Buchanan, J.C., and Tavana, H. Self-regulatory factors of embryonic stem cells in co-culture with stromal cells enhance neural differentiation. *Integr Biol (Camb)* **9**, 418, 2017.
56. Jin, K., Zhu, Y., Sun, Y., Mao, X.O., Xie, L., and Greenberg, D.A. Vascular endothelial growth factor (VEGF) stimulates neurogenesis in vitro and in vivo. *Proc Natl Acad Sci U S A* **99**, 11946, 2002.
57. Han, H.W., and Hsu, S.H. Chitosan derived co-spheroids of neural stem cells and mesenchymal stem cells for neural regeneration. *Colloids Surf B Biointerfaces* **158**, 527, 2017.
58. Sasai, Y. Cytosystems dynamics in self-organization of tissue architecture. *Nature* **493**, 318, 2013.
59. Achilli, T.M., McCalla, S., Tripathi, A., and Morgan, J.R. Quantification of the kinetics and extent of self-sorting in three dimensional spheroids. *Tissue Eng Part C Methods* **18**, 302, 2012.
60. Song, W., Tung, C.K., Lu, Y.C., *et al.* Dynamic self-organization of microwell-aggregated cellular mixtures. *Soft Matter* **12**, 5739, 2016.
61. De Francesco, F., Tirino, V., Desiderio, V., *et al.* Human CD34/CD90 ASCs are capable of growing as sphere clusters, producing high levels of VEGF and forming capillaries. *PLoS One* **4**, e6537, 2009.
62. Kelm, J.M., and Fussenegger, M. Microscale tissue engineering using gravity-enforced cell assembly. *Trends Biotechnol* **22**, 195, 2004.
63. Erlandsson, A., Brannvall, K., Gustafsdottir, S., Westermarck, B., and Forsberg-Nilsson, K. Autocrine/paracrine platelet-derived growth factor regulates proliferation of neural progenitor cells. *Cancer Res* **66**, 8042, 2006.
64. Hung, S.P., Yang, M.H., Tseng, K.F., and Lee, O.K. Hypoxia-induced secretion of TGF-beta1 in mesenchymal

- stem cell promotes breast cancer cell progression. *Cell Transplant* **22**, 1869, 2013.
65. Gao, L., Cen, S., Wang, P., *et al.* Autophagy improves the immunosuppression of CD4+ T Cells by mesenchymal stem cells through transforming growth factor-beta1. *Stem Cells Transl Med* **11**, 1495, 2016.
  66. Wang, L., Shi, J., van Ginkel, F.W., *et al.* Neural stem/progenitor cells modulate immune responses by suppressing T lymphocytes with nitric oxide and prostaglandin E2. *Exp Neurol* **216**, 177, 2009.
  67. Almalki, S.G., and Agrawal, D.K. Effects of matrix metalloproteinases on the fate of mesenchymal stem cells. *Stem Cell Res Ther* **7**, 129, 2016.
  68. Mittal, R., Patel, A.P., Debs, L.H., *et al.* Intricate functions of matrix metalloproteinases in physiological and pathological conditions. *J Cell Physiol* **231**, 2599, 2016.
  69. Bartosh, T.J., Ylostalo, J.H., Bazhanov, N., Kuhlman, J., and Prockop, D.J. Dynamic compaction of human mesenchymal stem/precursor cells (MSC) into spheres self-activates caspase-dependent IL1 signaling to enhance secretion of modulators of inflammation and immunity (PGE2, TSG6 and STC1). *Stem Cells* **31**, 2443, 2013.
  70. Liu, J., Gotherstrom, C., Forsberg, M., *et al.* Human neural stem/progenitor cells derived from embryonic stem cells and fetal nervous system present differences in immunogenicity and immunomodulatory potentials in vitro. *Stem Cell Res* **10**, 325, 2013.
  71. Santos, J.M., Camoes, S.P., Filipe, E., *et al.* Three-dimensional spheroid cell culture of umbilical cord tissue-derived mesenchymal stromal cells leads to enhanced paracrine induction of wound healing. *Stem Cell Res Ther* **6**, 90, 2015.
  72. Valente, M.M., Allen, M., Bortolotto, V., Lim, S.T., Conant, K., and Grilli, M. The MMP-1/PAR-1 axis enhances proliferation and neuronal differentiation of adult hippocampal neural progenitor cells. *Neural Plast* **2015**, 646595, 2015.
  73. Sart, S., Liu, Y., Ma, T., and Li, Y. Microenvironment regulation of pluripotent stem cell-derived neural progenitor aggregates by human mesenchymal stem cell secretome. *Tissue Eng Part A* **20**, 2666, 2014.
  74. Teixeira, F.G., Carvalho, M.M., Neves-Carvalho, A., *et al.* Secretome of mesenchymal progenitors from the umbilical cord acts as modulator of neural/glial proliferation and differentiation. *Stem Cell Rev* **11**, 288, 2015.
  75. Misumi, S., Kim, T.S., Jung, C.G., *et al.* Enhanced neurogenesis from neural progenitor cells with G1/S-phase cell cycle arrest is mediated by transforming growth factor beta1. *Eur J Neurosci* **28**, 1049, 2008.
  76. Wong, C.T., Ussyshkin, N., Ahmad, E., Rai-Bhogal, R., Li, H., and Crawford, D.A. Prostaglandin E2 promotes neural proliferation and differentiation and regulates Wnt target gene expression. *J Neurosci Res* **94**, 759, 2016.
  77. Zhang, Y., Liu, J., Yao, S., *et al.* Nuclear factor kappa B signaling initiates early differentiation of neural stem cells. *Stem Cells* **30**, 510, 2012.

Address correspondence to:

*Yan Li, PhD*

*Department of Chemical and Biomedical Engineering  
FAMU-FSU College of Engineering  
Florida State University  
2525 Pottsdamer Street  
Tallahassee, FL 32310*

*E-mail: yli@eng.fsu.edu*

*Teng Ma, PhD*

*Department of Chemical and Biomedical Engineering  
FAMU-FSU College of Engineering  
Florida State University  
2525 Pottsdamer Street  
Tallahassee, FL 32310*

*E-mail: teng@eng.fsu.edu*

*Received: September 22, 2017*

*Accepted: November 14, 2017*

*Online Publication Date: December 26, 2017*